IEEE Access
Multidisciplinary | Rapid Review | Open Access Journal

IEEE POWER & ENERGY SOCIETY SECTION

Received 30 March 2023, accepted 21 April 2023, date of publication 26 April 2023, date of current version 3 May 2023.

Digital Object Identifier 10.1109/ACCESS.2023.3270805

RESEARCH ARTICLE

Waveform Variation Defined Model for Harmonic Current Emissions Including Cross-Order Supply Voltage Harmonics Influence

KAMRAN DANIEL[1,2], (Graduate Student Member, IEEE), LAURI KÜTT[1], (Senior Member, IEEE), MUHAMMAD NAVEED IQBAL[1,3], NOMAN SHABBIR[4], (Senior Member, IEEE), MARTIN PARKER[1], AND MAREK JARKOVOI[1]

[1]Department of Electrical Power Engineering & Mechatronics, Tallinn University of Technology, 19086 Tallinn, Estonia
[2]Department of Electrical Engineering, University of Engineering and Technology, Lahore 54000, Pakistan
[3]Department of Electrical Engineering, GC University Lahore, Punjab 54000, Pakistan
[4]FinEST Center for Smart Cities, Tallinn University of Technology, 19086 Tallinn, Estonia

Corresponding author: Kamran Daniel (kdanie@taltech.ee)

This work was supported by the Estonian Research Council Grant PSG142.

ABSTRACT The paper reports an experimental non-linear load evaluation regarding current harmonics sensitivity to supply voltage harmonics. A base for the model is proposed relying on the time-domain waveform variations, rather than impedance or conductance approach. The proposed Waveform Variation Defined Model is able to detail to provide improved correspondence for the actual load physical operation on the emergence of cross-order coupling between the supply voltage and current harmonics variations. Model proposal specifies to implement non-impedance relation and separated phase and magnitude response components, in empirical outcome of the voltage-to-current harmonic variation relation. It will be shown that the model proposed is able to provide an accurate estimation on cumulative influence of different supply voltage harmonics included, for the most probable supply voltage harmonics in the residential grid, for the low order odd harmonics. Model results present outstanding match of the harmonic voltage influence estimations on the load current harmonics levels measured, phase and magnitude values included.

INDEX TERMS Power quality, current harmonic addition, harmonic estimation, harmonic sensitivity.

I. INTRODUCTION

This low voltage distribution network (DN) loads' harmonic current emissions are known to have a response to the harmonics present in the supply voltage [1], [2]. DNs are designed to supply constant RMS magnitude and frequency AC supply voltage with small tolerance around rated values in normal operation [3], [4]. However, as modern energy-efficient electrical devices utilize DC voltage for their operation, power input is commonly delivered by converting the mains AC voltage to DC voltage for power electronic (PE) units using full-bridge rectifiers [5].

In order to model the current waveform response of several power electronic loads in DN system, analysis is often performed in the frequency domain [6], [7], [8], assuming sinusoidal supply voltage. Harmonic current emission assumed as constant $\boldsymbol{I}_{\boldsymbol{h}}^{*} = I_{hM,const} \angle \varphi_{Ih,const}$ is one of the common presentations for harmonic [9], [10] fingerprinting. It faces clear limits for DN supply voltage having some voltage harmonic content, as an evident coupling/sensitivity emerges from measurements [11]. In the following paper, for the benefit of clarity, the current waveform harmonic components are nominated as vectors $\boldsymbol{I}_{\boldsymbol{x}}^{*}$, with "$x$" stating the current harmonic order observed; whereas supply voltage harmonic components are nominated as vectors $\boldsymbol{U}_{\boldsymbol{y}}^{*}$ with "y" stating the voltage harmonic order observed, if different form "x".

A Norton model employs two current harmonic components, a constant current source with current $\boldsymbol{I}_{\boldsymbol{x,Base}}^{*}$ and a linear impedance reaction $\boldsymbol{I}_{\boldsymbol{x,Z}}^{*}$ [12], [13]. $\boldsymbol{I}_{\boldsymbol{x,Base}}^{*}$ emerges as a constant value, upon non-distorted sinusoidal voltage supply. On a vector plot, Norton model proposes that the current

The associate editor coordinating the review of this manuscript and approving it for publication was Elisabetta Tedeschi.

emission of the device resides around an acceptable reference quantity, that is, an ideal sinusoidal voltage condition current emission (modeled as a constant current source) and is linear for minor deviations. If a voltage harmonic influence is represented by a vector $\boldsymbol{U}_x^* = U_{xM} \angle \varphi_{Ux}$, a response on the load's harmonic current would emerge as

$$I_{x,Z}^* = \frac{U_x \angle \varphi_{Ux}}{Z_x \angle \varphi_{zx}} \tag{1}$$

However, Norton model lacks the explanation on several aspects evident in the measurement results. It is unable to accurately present how a supply voltage harmonic of a specific order imposes variation on the current harmonic of another order (cross-order coupling) and is limited to describe the variations for different supply voltage levels.

As more sophisticated models for providing a multi-influence response forming the total $\boldsymbol{I}_{\boldsymbol{x,FCM}}^*$, frequency coupling matrix (FCM) is one of the most discussed models at the time [14]. Utilizing impedance or conductance values for accounting for influence arising from different voltage harmonic orders, the FCM addresses the Norton model circuit base approach and assumes the total $\boldsymbol{I}_{\boldsymbol{x,FCM}}^*$ arises from a cumulation of multiple sub-reactions. Using FCM, the x-th harmonic current vector could be written as

$$\boldsymbol{I}_{\boldsymbol{x}}^* = \boldsymbol{I}_{\boldsymbol{x,Base}} + [\boldsymbol{U}^*][\boldsymbol{Y}_{\boldsymbol{xy}}^*] \tag{2}$$

Here $[\boldsymbol{U}^*]$ is a supply voltage vector matrix, enclosing voltage harmonic component vectors of different harmonic orders, $[\boldsymbol{Y}_{\boldsymbol{xy}}^*]$ is the frequency coupling admittance matrix between the x-th harmonic current component and each y-th voltage harmonic component in $[\boldsymbol{U}^*]$ [15].

Challenges of FCM arise again as the modeling of practical devices in practical networks results in deviations. While the impedance-based products of harmonic voltage $\boldsymbol{U}_y^*$ phase influences are used, these are best to describe $\boldsymbol{I}_x^*$ circular vector plot result patterns [16]. However, $\boldsymbol{U}_y^*$ phase influence patterns are often elliptical in form (see also Chapter IV in this paper). It has been provided that to describe the elliptical result pattern, another set of variables should be included via negative-sequence FCM [6], [17], [18] or additional frequency component factor [19]. These make the FCM more heavy for calculation and parameter estimation. While the FCM would be capable of providing a current harmonic magnitude response, it does not include a direct physical phenomenon description for the harmonic cross-order coupling [14], [20], [21]. Remaining complexity and the deviation in $\boldsymbol{I}_x^*$ phase result will provide limitations of range for the FCM, as the cumulative assessment of total $\boldsymbol{I}_y^*$ different sub-reactions via (10) also means cumulation of deviations.

In this paper, a novel model is proposed for establishing a total $\boldsymbol{I}_x^*$ estimation model, able to include harmonic cross-coupling physical phenomenon and load current elliptical response reasons to $\boldsymbol{U}_y^*$ phase variation. It will be presented that due to physical phenomenon of the operation of the rectifier circuits; there is more optimal way of describing the time-difference reactions via separate time-difference/phase-difference coefficients and magnitude difference via separate magnitude difference coefficients. For the voltage waveform having the same harmonic RMS-value but a different harmonic phase angle value, the rectifier conduction initiation moment of the current waveform is unique, defining phase shift variation. Furthermore, the duration as well as the peak of the load current pulse are also dependent on the incident harmonic phase angle value. These coefficients would invalidate the total harmonic presentation through complex impedance variables.

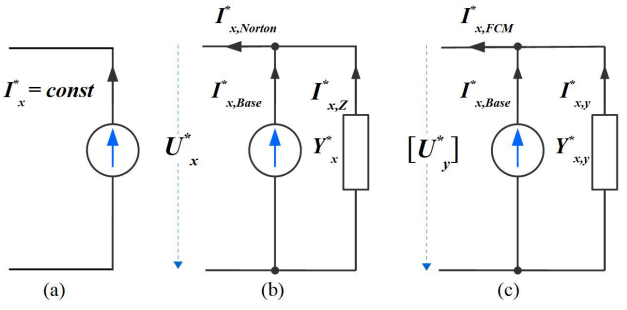

FIGURE 1. Harmonic load reaction models, (a) constant source (b) Norton equivalent (c) FCM [22], [23].

II. EXPERIMENTAL SETUP

The more detailed analysis of the loads $\boldsymbol{U}_y^*$ sensitivity relied on a systematic scan, similar to [24] and [25], performed on different loads exhibiting similar load current characteristics (load types, see further [26]). For the test system, dynamic high-resolution control of the waveform of supply voltage for measured load is a primary feature. Supply voltage is output through a high-precision amplifier, provided with reference from 16-bit waveform synthesizer, updated in every 10 seconds for different harmonic voltage content. The supply voltage output momentary value is established using equation (3).

$$u_{test}(t) = \sum_{y=1}^{N} \sqrt{2} U_y \sin\left(2\pi f_y t + \alpha_y\right) \tag{3}$$

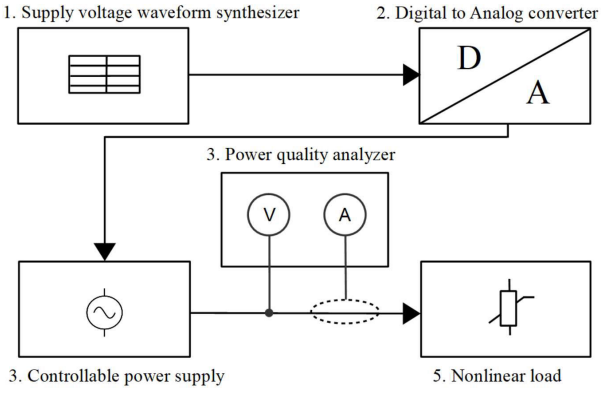

FIGURE 2. Measurement setup [27].

U_y is the rms value of any particular harmonic. The harmonic frequency is shown by f_y and sampling interval by t_s. The number of samples needed for the specific duration (T_m) of the voltage output from the controllable power supply can be calculated by (3).

Supply waveform is generated with the sampling frequency of 100 kS/s; meaning 2000 points for every 50 Hz cycle. Measurements are done via measurement unit having 41 kS/s sampling frequency, with waveform recordings and 1-second averaging of the harmonics used. Extracted values for current harmonics were recorded with a magnitude and phase response values, correlated to the waveform-sampled values.

Commencing the more detailed analysis several criteria was considered for more accurate measurements. First, time dependency of harmonic emission profiles of switch-mode power supplies (SWMPs) [28] was considered. Measurements are done only after the thermal stability of the load, warmup period 60 minutes was applied. Continuous power is provided to loads during testing pauses to maintain a working temperature [29].

During the characteristic scan of the loads, miniature though stable and repeatable variations of the harmonic current component phase and magnitude values were recorded. This was verified with discrete Fourier transform (DFT) of the current waveform. The measurement analyzer used in this study was commercially certified to carry out accurate and repeatable measurements of such order of level magnitude and phase angle variations [30].

Main load characteristics scan is done through scenarios such as presented in Table 1 for the 5th harmonic. As the first test supply voltage combination, the harmonic currents of the load are recorded for input voltage containing only the fundamental component U_1. After that, each input voltage combinations are present for 10 seconds. 24 combinations implement injection of voltage harmonic to the supply voltage, having identical 5th harmonic voltage U_5 level but phase angle at 15-degree steps. This was repeated with different level of influencer U_5 magnitude applied.

TABLE 1. An example of supply voltage combination when adding single harmonic to supply voltage.

Combinations	U^*_1	U^*_3		U^*_5		U^*_7	
	U_1, V	U_3, V	φ_{U3} °	U_5, V	φ_{U5} °	U_7, V	φ_{U7} °
1	230	0	0	0	0	0	0
24	230	0	0	3	0-15 …345	0	0

III. LOAD SCAN RESULTS

The LED lamps commercially available in the market are can be categorized based on the waveform of the drawn current by LED [26] shown in Fig. 3; the shape of the current waveform depend on the presence or absence of the waveform control or filter in the circuit of lamps [31], [32], [33], [34]. In this study, randomly chosen LED lamps of Type A [26] are observed, and evaluated for the odd harmonic contents and reaction for the harmonic orders 3, 5 and 7.

Starting with a time-domain observation, Figure 4 describes the current waveform as a LED lamp is subjected to pure sinewave supply voltage, compared to the supply voltage waveform having a specific harmonic voltage component magnitude level, injected with a specific phase angle towards the main harmonic phase. Figure 4 describes a selection of the current waveforms outcome of a scan result when 5th voltage harmonic was applied with a defined level, and the harmonic injection phase angle varied in 15-degree steps while the harmonic voltage level preserved (see Table 1). Measured

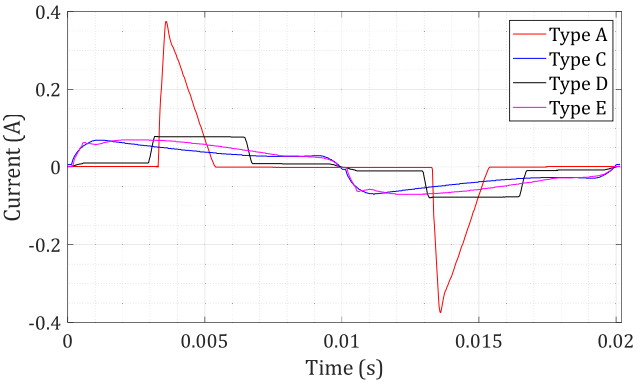

FIGURE 3. Load types of LED lamps tested.

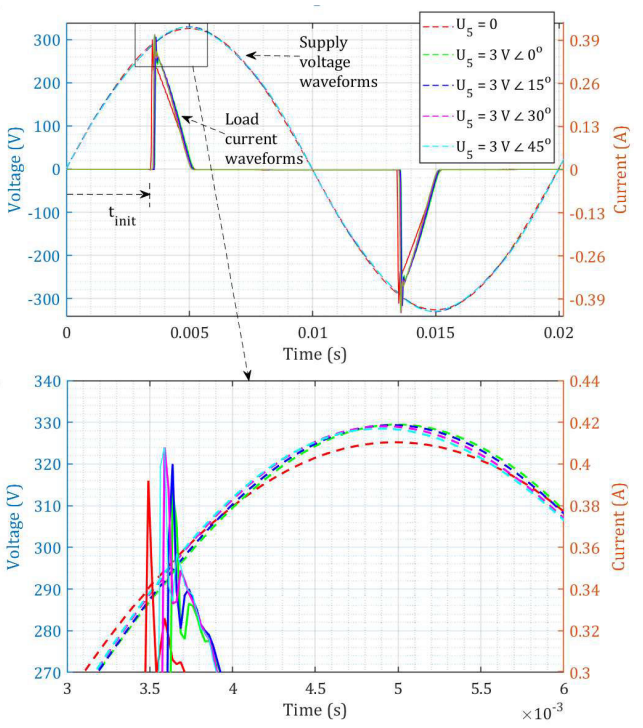

FIGURE 4. Current waveform initiation moment affected by the phase angle of 5th order supply voltage harmonic, measurement results. Dashed lines – supply voltage waveforms; continuous lines – load current waveforms.

current waveforms have been synchronized to the voltage waveform main harmonic zero phase instant.

A distinctive quantity of the current waveform is the point of rectifier conduction initiation time instant t_{init}. Here current provides highest gradient and peaks some moment later. The rectifier current instantaneous peaks provide a characteristic quantity for the magnitude, and another distinctive time-domain characteristic would be the total conduction time of the rectifier.

The current waveform of all the LEDs tested shows similar characteristics of response to voltage harmonics added to the input voltage. Fig. 4 shows the former effect, in terms of amplitude and phase angle of the harmonic current, and it is clear that change in phase angle of the fifth voltage harmonic affects the harmonic currents across the spectrum. The initiation moment given as main harmonic phase angle value (φ_{init}), could be seen to determine to deviation of the LED harmonic current pattern. Time-domain differences have been regarded towards phase angle variation in the literature [35], [36], however not used for base assumption.

The time domain outcome thus establishes a hypothesis if the initiation phase angle would be responsible for the LED current harmonic phase angle variations throughout. The hypothesis proposed refers that the current harmonic phase angles will be directly related to the rectifier physical operation in the time-domain.

IV. PHASOR PLOT PRESENTATION

Measurements thus directly have revealed that due to added voltage harmonics, there are influences to both current conduction initiation time instant (i.e., phase angle) and current magnitude values. For the detailed characterization of frequency approach, total $\boldsymbol{I}_x^*$ was recorded for supply voltage with the specific harmonic component constant magnitude, while rotating in smaller steps through the 360 degrees phase angle. Results present a well-reported [14], [18], [25], [37], [38], though less-approached outcome.

In the following, the harmonic current vector (example of $\boldsymbol{I}_7^*$ in plot Figure 5) difference to base point $\boldsymbol{I}_{7,Base}^*$ is observed as

$$\begin{cases} dI_{x,Uy} = I_{x,Uy} - I_{x,Base} \\ d\varphi_{Ix,Uy} = \varphi_{Ix,Uy} - \varphi_{Ix,\mathrm{Base}} \end{cases} \tag{4}$$

where $\mathrm{d}I_{x,Uy}$ is the measured harmonic current $\boldsymbol{I}_x^*$ magnitude difference due to included $\boldsymbol{U}_y^*$, compared to $\boldsymbol{I}_x^*$ magnitude $I_{x,Base}$ emerging in pure sinewave voltage supply conditions;

$\varphi_{Ix,Uy}$ is the measured harmonic current $\boldsymbol{I}_x^*$ phase angle due to included $\boldsymbol{U}_y^*$, compared to $\boldsymbol{I}_x^*$ phase angle $\varphi_{Ix,Base}$ emerging in pure sinewave voltage supply conditions.

Plot in Figure 5 presents the common measurement outcome for the influence of $\boldsymbol{U}_5^*$ added to the sinusoidal supply voltage, with φ_{U5} rotation applied for full circle (through 360°) and magnitude U_5 held constant. The response of $\boldsymbol{I}_7^*$ endpoints makes up an ellipse, but also $\varphi_{dI7,U5}$ is going through a rotation of exactly 360°. This is evident also for other all other current harmonics, regardless of their frequency value.

While linear impedance can explain the current difference component phase rotation, this is only valid for the harmonic of same order, i.e., identical frequency. As this emerges for all harmonics, for example added $\boldsymbol{U}_3^*$ rotated through $\varphi_{U3} = \{0 \ldots 360°\}$ again provides $\varphi_{dI7,U3}$ rotation through 360°, then this cannot be considered an impedance-based relation. This will follow the coefficient proposals for model for calculating the harmonic current values.

It emerges that reaction plot is rather well symmetrical towards the pure-sinusoidal voltage supply product of $\boldsymbol{I}_x^*$, termed here as the base harmonic current response $\boldsymbol{I}_{x,Base}^*$. Response towards both phase and magnitude response is proportional to the voltage harmonic influencer magnitude value I_{hM}. It raises the model description to the response as

$$\begin{cases} I_x = I_{x,\mathrm{base}} + \Delta I_{x,y} \\ \varphi_{Ix} = \varphi_{Ix,\mathrm{base}} + \Delta\varphi_{Ix,y} \end{cases} \tag{5}$$

where $\Delta I_{x,y}$ is the harmonic current $\boldsymbol{I}_x^*$ magnitude variation estimation due to included $\boldsymbol{U}_y^*$, compared to $\boldsymbol{I}_x^*$ magnitude $I_{x,Base}$ emerging in pure sinewave voltage supply conditions;

$\Delta\varphi_{Ix,y}$ is the is the harmonic current $\boldsymbol{I}_x^*$ phase angle magnitude estimation due to included $\boldsymbol{U}_y^*$, compared to $\boldsymbol{I}_x^*$ phase angle $\varphi_{Ix,Base}$ emerging in pure sinewave voltage supply conditions.

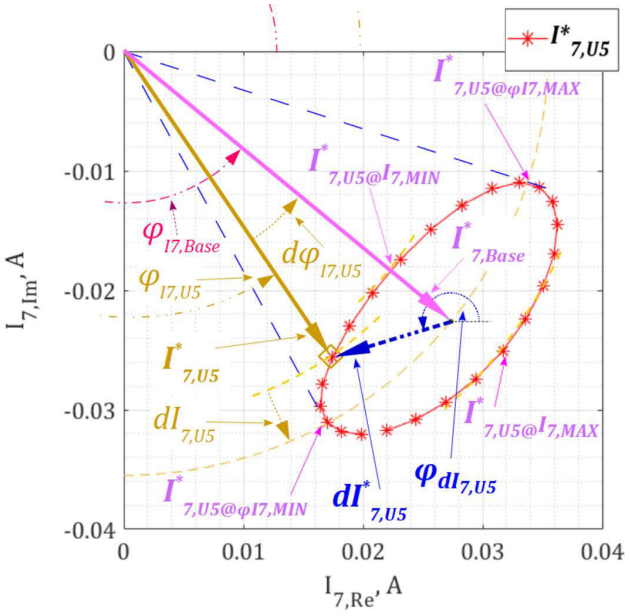

FIGURE 5. Vector component plot for the harmonic load current component analysis. $\boldsymbol{I}_7^*$ vector endpoints' ellipse points plot, for $\boldsymbol{U}_5$ = 3 V, φ_{U5} = 0, 15, 30 ...345°.

This presentation is following the basic Norton or FCM concepts. However, for the reasons laid out in the following chapter, and relying on the physical rectifier operation phenomenon, it is justified to keep the magnitude and phase

variation quantities independent rather than confined through complex impedance relation.

A. CURRENT HARMONIC PHASE ANGLE VARIATIONS

The initiation angle of the current conduction (φ_{init}) is a time instance where the rectifier starts to conduct for charging the tank capacitor after the rectifier. This initiation angle is determined as

$$\varphi_{init} = f \cdot 360^{o} \cdot \mathrm{d}t_{init} \tag{6}$$

where $\mathrm{d}t_{init}$ – time-difference of the supply voltage main harmonic zero phase instant and current conduction initiation moment. Shown in Table 2, initiation phase is referred to varying $\boldsymbol{U_5^*}$ added to the voltage supply. Measurement results in Table 2 present the summary of the results, where

$$\begin{cases} d\varphi_{init,Uy} = \varphi_{init,Uy} - \varphi_{init,\mathrm{base}} \\ d\varphi_{Ix,Uy} = \varphi_{Ix,Uy} - \varphi_{Ix,\mathrm{base}} \end{cases} \tag{7}$$

where $\varphi_{init,Uy}$ is the initiation moment phase with $\boldsymbol{U}*_{\boldsymbol{y}}$ injected to the supply voltage; $\varphi_{Ix,Uy}$ is the phase angle of the response current vector with $\boldsymbol{U}*_{\boldsymbol{y}}$ injected to the supply voltage, and "$_{Base}$" notates the values upon sinusoidal supply voltage conditions (i.e., only fundamental voltage component present).

TABLE 2. Initiation moment and phase angles of harmonics in load current, for different magnitude levels of harmonic voltage*.

U_5, V	φ_{U5}, °	$\varphi_{init,0}$, ° (50 Hz phase value)	φ_{I1}, °	φ_{I3}, °	φ_{I5}, °	φ_{I7}, °
0	–	62.1	18.0	231.6	87.2	304.2
		$\Delta\varphi_{init}$, °	$\Delta\varphi_{I1}$, °	$\Delta\varphi_{I3}$, °	$\Delta\varphi_{I5}$, °	$\Delta\varphi_{I7}$, °
1	180	–0.9	0.6	2.0	3.6	5.5
	345	1.1	–0.8	–2.5	–4.2	–6.2
3	180	–2.9	2.0	6.5	11.5	17.7
	345	2.9	–2.4	–6.9	–11.8	–17.4
5	180	–4.7	3.6	11.3	20.4	32.0
	345	4.6	–3.6	–10.7	–18.3	–26.8

* Phase angle accuracy/resolution has been provided for more detailed comparison

TABLE 3. Difference in Phase Angles of Harmonics in Load Current, For Different Magnitude Levels of Harmonic Voltage, determined by (9).

U_5, V	φ_{U5}, °	φ_{init}, °	$\Delta\varphi_{init}$, °	$\Delta\varphi'_{I1,U5}$, °	$\Delta\varphi'_{I3,U5}$, °	$\Delta\varphi'_{I5,U5}$, °	$\Delta\varphi'_{I7,U5}$, °
0	-	62.1					
1	180	61.2	0.9	-0.7	-0.7	-0.7	-0.8
	345	63.2	-1.1	0.8	0.8	0.8	0.9
3	180	59.2	2.9	-2.1	-2.2	-2.3	-2.5
	345	65.0	-2.9	2.3	2.3	2.4	2.5
5	180	57.4	4.7	-3.6	-3.8	-4.1	-4.6
	345	66.7	-4.6	3.5	3.6	3.7	3.8

* Phase angle accuracy/resolution has been provided for more detailed comparison

TABLE 4. Maximum and minimum of peak load current ($I_{L\,Peak}$) according to φ_{u5}.

U_5, V	φ_{U5}, °	$I_{L\,Peak}$, A	$\Delta I_{L\,Peak}$, A	$\Delta I_{1,U5}$, mA	$\Delta I_{3,U5}$, mA	$\Delta I_{5,U5}$, mA	$\Delta I_{7,U5}$, mA
0	-	0.40					
1	270	0.38	0.02	0.05	0.30	0.67	1.13
	90	0.42	-0.02	-0.06	-0.28	-0.73	-1.19
3	270	0.34	0.06	0.21	0.83	1.74	3.0
	90	0.45	-0.06	-0.06	-0.76	-2.05	-3.5
5	255	0.30	0.10	0.29	1.50	3.8	6.3
	105	0.49	-0.10	-0.25	-1.21	-3.1	-5.1

Normalizing the phase angles towards the initiation influencing component $\boldsymbol{U_5^*}$, and observing the relation towards the current harmonic $\boldsymbol{I_x}$ of order x, it is revealed to have a ratio of closely common to

$$\Delta\varphi'_{I_{x,Uy}} = \Delta\varphi_{init,Uy} \cdot x \cdot k_{WF} \tag{8}$$

where k_{WF}– waveform coefficient, with almost same value for the discussed current harmonic orders ($x = 3, 5, 7$). The initiation phase angle φ_{init} is in direct and proportional ratio to the φ_{I1}, resulting from a frequency domain transfer of t_{init} (φ_{init}). The statement above reveals that the variation of harmonic current phase angles, observed due to $\boldsymbol{U_5^*}$, is directly relational and proportional to the initiation angle φ_{init}.

It is important to point out that the harmonic phase angle values are all varying, if the voltage harmonic phase angle is varying. This is a key aspect to explain the harmonic cross-coupling phenomenon, considering that the phase angle variation of the $\boldsymbol{U_y^*}$ of a specific order will bring along a dedicated response to current harmonic phase angle of another order.

Table 3 presents the maximum and minimum value of initiation moment of the current waveforms, corresponding to φ_{U5} value extreme points, calculated as

$$\Delta\varphi'_{I_{x,y}} = \frac{\Delta\varphi_{Ix,y}}{x} \tag{9}$$

where x is the current harmonic order, further confirming the equation (8). Furthermore, the fundamental current harmonic component phase variation defines phase variations for all other load harmonics, given through fundamental component phase shift multiplied by the observed harmonic current order number. It has to be noted that the magnitude of the incident voltage harmonic (U_5) provides a proportional impact on the initiation moment and the $\boldsymbol{I_x^*}$ phase angle φ_{Ix} variation range. The phase angles are seen to pose a high and low value responsive to φ_{U5} rotation of almost 180°.

B. CURRENT HARMONIC MAGNITUDE VARIATIONS

Similarly, the highest value of the load currents ($I_{x,y,max}$) is also linked with the phase angle of influencing supply voltage harmonic (φ_{Uy}) on almost 180° rotation. Table 3 illustrates the behavior of time-domain waveform $I_{L,peak}$, corresponding

to φ_{U5}, providing maximum and minimum $\boldsymbol{I_x^*}$ magnitude I_x values with value range shown. It has to be noted, that the highest and lowest current magnitude occurrence are also found at nearly orthogonal (90°) values towards the φ_{U5} value for peak and minimum φ_{Ix} variation values.

Table 4 presents expectedly, that the harmonic magnitudes are directly proportional to the level of the added voltage harmonic (in this case it is $\boldsymbol{U_5^*}$). The proportion origins are evident from time-domain waveform peak current levels, deployed to the current harmonics observed, presenting a physical background for the cross-order harmonic coupling appearance for the magnitude portion.

V. MODEL OF HARMONIC RESPONSE CURRENTS CHARACTERIZATION OF PRACTICAL LOADS

Provided the phase angle and magnitude variation consideration in the previous chapter, it has to be pointed out that the physical characterization to the time-domain origins of the $\boldsymbol{I_x^*}$ components provides justification to model the phase angle φ_{Ix} and magnitude portions I_x independent of each other. This is due to non-impedance origins of the $\boldsymbol{I_x^*}$ variations in time-domain current presentation, discussed in previous chapter.

In the following, a load current model will be described, providing the correspondence of the current harmonic variations, detailed in the previous chapter. The load current harmonic vector $\boldsymbol{I_x^*}$ for a particular harmonic order x is formed of following parts (see also Figure 6):

1. A constant current source part of the harmonic current, $\boldsymbol{I_{x,Base}^*}$ respective for current magnitude component $I_{x,Base}$, and the current phase angle component $\varphi_{Ix,Base}$. This is the value obtained from device test with pure sinusoidal supply voltage.
2. A linear current component part $\Delta\boldsymbol{I_{x,LIN}^*}$, respective for current magnitude component $\Delta I_{x,LIN}$, and the current phase angle component $\Delta\varphi_{Ix,LIN}$. These are calculated as a cumulation of all linear components due to each $\boldsymbol{U_y^*}$ in the supply voltage, for every $\boldsymbol{I_x^*}$.
3. A nonlinear current component part $\Delta\boldsymbol{I_{x,NL}^*}$, respective for current magnitude component $\Delta I_{x,\mathrm{NL}}$, and the current phase angle component $\Delta\varphi_{Ix,\mathrm{NL}}$. The nonlinear part emerges from the fact that the current harmonic response on the ellipse is non-symmetrical. These parts are calculated as a cumulation of all linear components due to each $\boldsymbol{U_y^*}$ in the supply voltage, for every $\boldsymbol{I_x^*}$.

The load harmonic current will be presented as

$$\begin{cases} I_{x,WVDM} = I_{x,\mathrm{Base}} + \Delta I_{x,LIN} + \Delta I_{x,NL} \\ \varphi_{Ix,WVDM} = \varphi_{Ix,\mathrm{Base}} + \Delta\varphi_{Ix,LIN} + \Delta\varphi_{Ix,NL} \end{cases} \tag{10}$$

The main proportion of the current harmonic variation will be provided by the linear part, calculated as

$$\Delta I_{x,LIN} = \boldsymbol{U_y} \cdot \boldsymbol{G_x} \cdot \cos(\boldsymbol{\alpha_x} - \boldsymbol{\varphi_{Uy}}), \tag{11}$$

where $\boldsymbol{U_y}$ is the $\boldsymbol{U_y^*}$ magnitude matrix in form

$$\boldsymbol{U_y} = [U_3\ U_5\ \ldots\ U_N]$$

$\boldsymbol{G_x}$ is the current harmonic I_x magnitude sensitivity coefficient matrix in form

$$\boldsymbol{G_x} = \begin{bmatrix} G_{x3} \\ G_{x5} \\ \ldots \\ G_{xN} \end{bmatrix}$$

where G_{x3} presents I_x sensitivity to the 3rd supply voltage harmonic magnitude U_3 respectively, (units A/V = S), and

$$\cos(\boldsymbol{\alpha_x} - \boldsymbol{\varphi_{Uy}}) = \begin{bmatrix} \cos(\alpha_{x3} - \varphi_{U3}) \\ \cos(\alpha_{x5} - \varphi_{U5}) \\ \ldots \\ \cos(\alpha_{xN} - \varphi_{UN}) \end{bmatrix},$$

where α_{x3} is the specific phase coefficient for calculating I_x related to φ_{U3}, latter presenting the supply voltage harmonic $\boldsymbol{U_3^*}$ actual phase angle value.

Similarly, the main current harmonic phase angle variation will be provided by the linear part, calculated as

$$\Delta\varphi_{Ix,LIN} = \boldsymbol{U_y} \cdot \boldsymbol{k_x} \cdot \sin(\boldsymbol{\alpha_x} - \boldsymbol{\varphi_{Uy}}), \tag{12}$$

$\boldsymbol{k_x}$ is the current harmonic $\boldsymbol{I_{x,LIN}^*}$ phase angle $\Delta\varphi_{Ix}$ sensitivity coefficient matrix in form

$$\boldsymbol{k_x} = \begin{bmatrix} k_{x3} \\ k_{x5} \\ \ldots \\ k_{xN} \end{bmatrix}$$

where k_{x3} presents $\Delta\varphi_{Ix}$ sensitivity to the 3rd supply voltage harmonic magnitude U_3 respectively, (units °/V), and

$$\sin(\boldsymbol{\alpha_x} - \boldsymbol{\varphi_{Uy}}) = \begin{bmatrix} \sin(\alpha_{x3} - \varphi_{U3}) \\ \sin(\alpha_{x5} - \varphi_{U5}) \\ \ldots \\ \sin(\alpha_{xN} - \varphi_{UN}) \end{bmatrix}.$$

Here the coefficients G_{xy}, k_{xy} and α_{xy} are determined through load measurements, presented in the next chapter.

The nonlinear part of current will be calculated for supply voltage harmonic components as

$$\Delta I_{x,NL} = \boldsymbol{U_y} \cdot \left[\boldsymbol{A_{1m}} \sin\left(\boldsymbol{\varphi_{Uy}} + \boldsymbol{C_{1m}}\right) + \boldsymbol{A_{2m}} \sin\left(\boldsymbol{2\varphi_{Uy}} + \boldsymbol{C_{2m}}\right)\right] \tag{13}$$

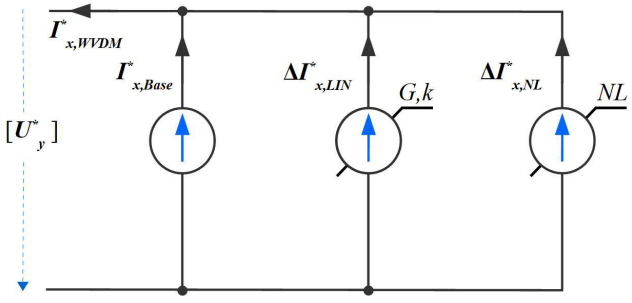

FIGURE 6. Schematic description for harmonic current component $\boldsymbol{I_x^*}$ of order x modeling.

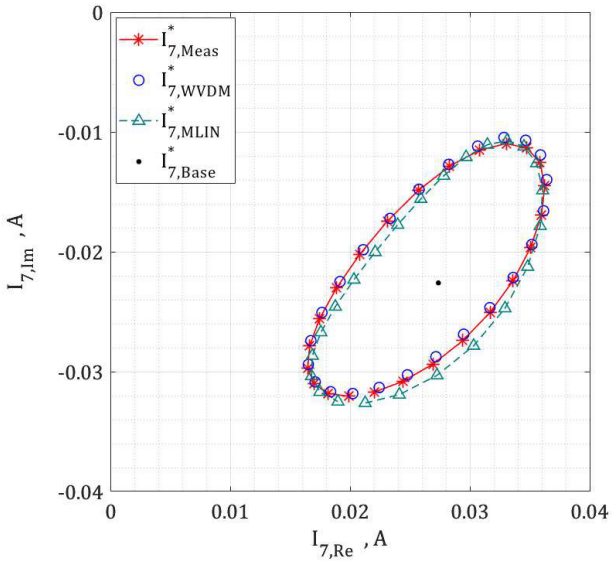

FIGURE 7. Presentation of roles of different harmonic current model components.

where A_{1m}, A_{2m}, C_{1m}, C_{2m} are first and second order polynomial expressions related to harmonic current order and harmonic voltage orders. Similarly nonlinear part for phase angle part will be calculated as

$$\Delta\varphi_{Ix,NL} = U_y \cdot \left[A_{1p} \sin\left(\varphi_{Uy} + C_{1p}\right) + A_{1p} \sin\left(1\varphi_{Uy} + C_{1p}\right)\right] \tag{14}$$

where $A_{1p}, A_{2p}, C_{1p}, C_{2p}$ are second order polynomial expressions related to harmonic current order and harmonic voltage orders.

The particular derivation of the polynomials as calculation of the nonlinear parts will be presented in further upcoming papers by the authors, as this will need extended consideration.

The role of the different components shown here are laid out in Figure 7 below. The main base of the harmonic current vector, $I^*_{7,Base}$ is presented with a dot as the vector endpoint, while its start-point is zero coordinate, corresponding to load current upon pure sinusoidal supply voltage. Red asterisks are forming a presentation of measured harmonic current results, subjected to supply including a single harmonic voltage U^*_5, included with various phase angles $\Delta\varphi_{U5}$ but identical magnitude. Adding the linear parts ΔI_7 and $\Delta\varphi_{I7}$ make up a pattern represented by triangles, forming a specific ellipse shape. Still, there would be a noticeable deviation between the linear-part-included harmonic current results and measurement results. Therefore, the nonlinear part is added to provide improved correspondence to the actual measurement outcome. The final harmonic current response pattern, including the linear and nonlinear parts, is presented as circles' pattern.

VI. DETERMINATION OF COEFFICIENTS

In the following, the main outline will be discussed for the coefficient estimation, used in the harmonic current calculation model. An example of I^*_7 current component will be used, influenced by the effect of the U^*_5 supply voltage harmonic. Here $x = 7$ is the current harmonic order, $y = 5$ is influencing voltage harmonic order. The quantities observed are referred to on the basis of Figure 5.

Ideally, for ΔI_x to reach from $\Delta I_{x,MAX}$ to almost equal to zero, i.e., current vector magnitude is similar to the sinusoidal supply voltage component response vector $\Delta I_{x,Base}$, base harmonic vector; the difference in φ_{Uy} is nearly 90 degrees. At the voltage harmonic phase angle providing harmonic current I_x of base magnitude, the φ_{Ix} phase deviation is highest. Finding the influencing supply voltage phase angles φ_{Uy} corresponding to the minimum and maximum deviation of the magnitude I_x, allows to specify the base phase shift component

$$\alpha_{xy} = \frac{\varphi_{Uy@\varphi Ix,MAX} + \varphi_{Uy@\varphi Ix,MIN}}{2} \tag{15}$$

referring to measurement quantities as in Figure 5. Given the data provided in Table 5, the α_{75} is found to be close to value of 230°. As the measurement steps are 15°, better accuracy is not available. Given the orthogonal shift of $\varphi_{Uy} = 90°$ to find the maximum and minimum magnitude points, the α_{75} should be calculated as

$$\alpha_{xy} = \frac{\varphi_{Uy@Ix,MAX} + \varphi_{Uy@Ix,MIN}}{2} + 90° \tag{16}$$

Data in Table 5 provides that the α_{75}, calculated based on minimum and maximum magnitude, will be around 240°. The proposed value of coefficient of current magnitude sensitivity G_{xy} can be found using maximum and minimum I^*_x magnitude difference value i.e., dI_x maximum and minimum values (referring to Figure 5)

$$G_{xy} = \frac{\left(\left|dI_{x,Uy@Ix,MAX}\right| - \left|dI_{x,Uy@Ix,MIN}\right|\right)}{U_y} \tag{17}$$

TABLE 5. Proposing Alpha Value Form Measurements.

		φ_{U5}	$\varphi_{U5\_MAX} - \varphi_{U5\_MIN}$	φ_{U5_CENTRE}	α_{75} for $dI_7 \approx 0$	α_{75}
dI_{7_MAX}	6.6 mA	225°	-150°	150°	240°	233°
dI_{7_MIN}	-4.9 mA	75°				
$d\varphi_{I7\_MAX}$	21.7°	315°	-165°	233°	233°	
$d\varphi_{I7\_MIN}$	-21.5°	150°				

TABLE 6. Comparison Of Voltage Harmonic Amplitude Change To Current Harmonic Phase Deviation.

Load	U_5	K_{35}, °/V	G_{35}, mA/V	K_{55}, °/V	G_{55}, mA/V	K_{75}, °/V	G_{75}, mA/V
1	1 V	3.17	0.22	5.3	0.63	7.5	1.08
	3 V	3.16	0.23	5.3	0.65	7.6	1.11
	5 V	3.16	0.27	5.3	0.70	7.5	1.14

TABLE 7. Model Parameters of Test Loads.

	I_x order	3			5			7		
U_y order	Load	α_{3y}, °	G_{3y}, mA/V	k_{3y}, °/V	α_{5y}, °	G_{5y}, mA/V	k_{5y}, °/V	α_{7y}, °	G_{7y}, mA/V	k_{7y}, °/V
3		25	0.07	2.16	26	0.18	3.6	28	0.39	5.1
5	1	218	0.24	3.2	220	0.67	5.3	223	1.13	7.5
7		48	0.51	3.6	52	1.22	6.2	57	1.96	8.9
3		29	0.12	2.12	31	0.42	3.6	35	0.75	5.1
5	2	223	0.51	2.95	226	1.27	5.0	233	1.91	7.3
7		53	0.92	3.1	59	2.06	5.4	71	3.03	8.1
3		28	0.10	2.13	29	0.31	3.6	32	0.60	5.1
5	3	221	0.39	2.99	224	1.01	5.1	229	1.58	7.3
7		512	0.74	3.3	57	1.69	5.6	66	2.57	8.3

TABLE 8. Comparison of measured and model calculated Harmonic current values $U_1 = 230$ V; $U_5 = 3$ V.

I/P	*Measured values*				*Model with linear part result*				*Deviation for model with linear part*		*Full model result*		*Full model deviation from measurement*	
φ_{U5}, °	$I_{7,MEAS}$, mA	$\varphi_{I7,MEAS}$, °	$dI_{7,MEAS}$, mA	$d\varphi_{I7,MEAS}$, °	$\Delta I_{7,MLIN}$, mA	$\Delta\varphi_{I7}$, °	$I_{7,MLIN}$, mA	$\varphi_{I7,MLIN}$, °	$\delta I_{x,MLIN}$, mA	$\delta\varphi_{Ix,MLIN}$, °	$I_{7,WVDM}$, mA	$\varphi_{I7,WVDM}$, °	$\delta I_{x,WVDM}$, mA	$\delta\varphi_{Ix,WVDM}$, °
Max	40.4	-18	6.5	21.7	5.7	21.6	41.2	-18	1.8	1.7	40.3	-17	0.4	-0.2
Min	29.0	-61	-4.9	-21.5	-5.7	-21.6	29.8	-61	-1.0	-3.1	29.0	-61	0.0	-1.0
75	40.4	-34	-4.9	-5.8	-5.3	-8.1	40.8	-31	-0.4	-2.3	40.3	-33	0.1	-0.3
150	36.6	-18	-1.1	-21.5	0.7	-21.6	34.8	-18	1.8	-0.1	36.3	-17	0.3	-0.9
225	29.0	-37	6.5	-2.6	5.7	-3.0	29.8	-37	-0.9	-0.5	29.0	-36	0.0	-0.6
315	35.4	-61	0.1	21.7	0.8	21.5	34.7	-61	0.7	-0.2	35.3	-61	0.1	-0.3
RMS error for 24 U_5 phase angles injected									**0.9**	**2.1**			**0.2**	**0.5**

From the result plots (Figure 5, Figure 7) it is evident that base harmonic current vector $\boldsymbol{I^*_{x,Base}}$ does not lie in the centre of ellipse, and with the non-symmetric part included, the average of $|dI_{x,y@Ix,MAX}|$ and $|dI_{x,y@Ix,MIN}|$ is used to determine the G_{xy} using equation (17). The phase variation margins are well symmetrical to the ellipse centre, and to determine the initial proposed value of coefficient of phase angle change (k_{xy}), the measurement-derived $d\varphi_{Ix,Uy@\varphi Ix,MAX}$ is used as in (18)

$$k_{xy} = \frac{d\varphi_{Ix,Uy@\varphi Ix,MAX}}{U_y} \tag{18}$$

The magnitude of the harmonic current difference vectors is linearly dependent on the U_y. This way, for influencer U_5 increase by 3 (from 1 V to 3 V) times, results emerge for the $d\varphi_{Ix,Uy@\varphi Ix,MAX}$ and similarly $dI_{x,Uy@Ix,MAX}$ and $dI_{x,Uy@Ix,MIN}$ that provide the close values of linear scalar coefficients G_{xy} and k_{xy}. Excellent linearity of the coefficients is evident from Table 6. Using presented procedures in (15),(16) and (18) the linear coefficients for different loads discussed further in this paper are presented in Table 7.

VII. SINGLE SUPPLY VOLTAGE HARMONIC COMPONENT MODELING

For more detailed evaluation, the linear component model results are presented for 3 similar type loads. Main emphasis is on the comparison of the measured vs model calculated results. Coefficients from Table 7 have been implemented for the model calculation with linear part included (see (10)), as

$$\boldsymbol{I_{x,MLIN}} = \boldsymbol{I_{x,Base}} + \boldsymbol{\Delta I_{x,LIN}} \tag{19}$$

$$\boldsymbol{\varphi_{Ix,MLIN}} = \boldsymbol{\varphi_{Ix,Base}} + \boldsymbol{\Delta\varphi_{Ix,LIN}} \tag{20}$$

Deviation of calculation to measured magnitude value is presented as

$$\boldsymbol{\delta I_{x,LIN}} = \left|\boldsymbol{I_{x,Meas}}\right| - \left|\boldsymbol{I_{x,Base}} + \boldsymbol{\Delta I_{x,LIN}}\right|, \tag{21}$$

and similarly

$$\boldsymbol{\delta\varphi_{Ix,LIN}} = \left|\boldsymbol{\varphi_{Ix,Meas}}\right| - \left|\boldsymbol{\varphi_{Ix,Base}} + \boldsymbol{\Delta\varphi_{Ix,LIN}}\right|, \tag{22}$$

where $\delta I_{x,LIN}$ presents the magnitude difference of model (see (10)) result without nonlinear part included, compared to measurement outcome;

$\delta\varphi_{Ix,LIN}$ presents the phase difference of model (see (10)) result without nonlinear part included, compared to measurement outcome.

The full model calculation outcome, including the nonlinear part is calculated according to (10). The deviation between the full model calculation and measurement outcome is calculated as

$$\boldsymbol{\delta I_{x,WVDM}} = \left|\boldsymbol{I_{x,Meas}}\right| - \left|\boldsymbol{I_{x,WVDM}}\right|, \tag{23}$$

TABLE 9. Difference Of Measurement And Estimation For Test Loads; Single supply harmonic $U_5 = 3$ V.

Load		I^*_3						I^*_5						I^*_7					
		$I_{3,MEAS}$, mA	$I_{3,MLIN}$, mA	$I_{3,WVDM}$, mA	$\varphi_{I3,MEAS}$, °	$\varphi_{I3,MLIN}$, °	$\varphi_{I3,WVDM}$, °	$I_{5,MEAS}$, mA	$I_{5,MLIN}$, mA	$I_{5,WVDM}$, mA	φ_{I5_MEAS}, °	$\varphi_{I5,MLIN}$, °	$\varphi_{I5,WVDM}$, °	$I_{7,MEAS}$, mA	$I_{7,MLIN}$, mA	$I_{7,WVDM}$, mA	$\varphi_{I7,MEAS}$, °	$\varphi_{I7,MLIN}$, °	$\varphi_{I7,WVDM}$, °
1	Max	40.4	40.5	40.4	-118	-119	-118	36.3	36.8	36.4	103	103	104	31.0	31.7	31.0	-32	-32	-32
	Min	38.9	39.0	39.0	-137	-137	-137	32.3	32.8	32.4	72	72	72	24.2	24.9	24.4	-78	-78	-77
	RMSE		**0.3**	**0.1**		**0.9**	**0.1**		**0.5**	**0.1**		**1.3**	**0.2**		**0.6**	**0.1**		**2.0**	**0.4**
2	Max	59.4	59.7	59.6	-114	-114	-114	51.0	51.7	51.1	112	112	113	40.4	41.2	40.3	-18	-18	-17
	Min	56.4	56.7	56.5	-131	-131	-131	43.4	44.2	43.6	82	82	83	29.0	29.8	29.0	-61	-61	-61
	RMSE		**0.6**	**0.1**		**1.0**	**0.2**		**0.8**	**0.1**		**1.6**	**0.2**		**0.9**	**0.2**		**2.1**	**0.5**
3	Max	50.8	51.0	51.0	-117	-117	-117	44.3	44.9	44.4	106	106	107	35.9	36.7	35.8	-27	-27	-26
	Min	48.5	48.7	48.6	-135	-135	-135	38.3	38.9	38.4	76	76	76	26.5	27.2	26.5	-70	-70	-70
	RMSE		**0.5**	**0.1**		**1.0**	**0.1**		**0.7**	**0.1**		**1.5**	**0.2**		**0.8**	**0.2**		**2.1**	**0.4**

and similarly

$$\delta\varphi_{Ix,WVDM} = \left|\varphi_{Ix,Meas}\right| - \left|\varphi_{Ix,WVDM}\right|. \tag{24}$$

For the whole $\boldsymbol{U}^*_y$ cycle (360°) rotation the outcome deviation is evaluated using the root-mean-square error (RMSE), listed in tables 8 and 9 is calculated using the following equations,

$$RMSE_{Ix} = \sqrt{\frac{\sum_{i=0}^{N} \delta \boldsymbol{I}_x{}^2}{N}} \tag{25}$$

$$RMSE_{\varphi Ix} = \sqrt{\frac{\sum_{i=0}^{N} \delta\varphi_{Ix}{}^2}{N}} \tag{26}$$

where N_{MEAS} is total number of actual (measurement) points and predicted values (magnitude and phase).

Individual results obtained with model linear part results are rather accurate (Table 8), however, if considering the variation full amplitude of 5.7 mA, the maximum model linear part deviation reaches 1.8°, which is roughly 30% of the full variation amplitude. While good for single harmonic voltage component influence estimation, it will be shown in the following chapters that for the cumulative multiple voltage harmonics influence model to have reasonable outcome, the single harmonic voltage influence would need to have as good correspondence as possible. Thus, the nonlinear part included full model (see (10)) calculation can provide very low RMSE value (Table 8). This is valid for multiple loads tested (see Table 9) where the correspondence between the measured and model calculated values shows very high match.

VIII. CUMULATIVE RESPONSE TO VOLTAGE HARMONICS

The harmonic current calculation model (10) is referred through parts (11, 12) that are making up a scalar product of multiple influences from supply voltage harmonics of different order. This means that the model is able to account for cumulative sum of influences on the harmonic current $\boldsymbol{I}^*_x$ from multiple supply voltage harmonic components. In order to present this, a measurement based cumulative influence

TABLE 10. Input-Combination-2 When Adding Multiple Harmonic Voltages to Fundamental Voltage.

No. of supply voltage combinations applied	U^*_1	U^*_3		U^*_5		U^*_7	
	U_1, V	U_3, V	φ_{U3} °	U_5, V	φ_{U5} °	U_7, V	φ_{U7} °
1	230	0	0	0	0	0	0
24	230	3	0-15-345	0	0	0	0
24	230	3	120	3	0-15-345	0	0
24	230	3	315	3	0-15-345	0	0

analysis is presented. In trivial, the cumulative response is approached in a manner to keep one or multiple supply voltage harmonics as constant vectors while the single other order harmonic voltage component $\boldsymbol{U}^*_y$ is rotated through 360°, keeping the magnitude U_y constant.

Staring with initial base harmonic current $\boldsymbol{I}^*_{7,base}$ point ("1" in Figure 8, sinusoidal supply voltage conditions), $\boldsymbol{U}^*_3$ is first applied. The rotation of the $\boldsymbol{U}^*_3$ provides an ellipse common from the previous chapters (see Figure 8, black line and asterisks). Two extreme points of attention have been selected next, having $\boldsymbol{I}^*_7$ with minimum ("2" in Figure 8) and maximum phase value ("3" in Figure 8). Next, using $\boldsymbol{U}^*_3$ respective to the point of interest on graph, $\boldsymbol{U}^*_5$ is added and rotated through 360°. Results have been reported as further ellipses, having their center-points in the points of interest previously identified. Therefore, the geometrical cumulation of influence vectors due to different harmonic orders of supply voltages included, can be directly observed. Here even cumulation of $\boldsymbol{U}^*_3$ and $\boldsymbol{U}^*_5$ can be seen to provide up to 80° $\boldsymbol{I}^*_7$ rotation. The points of $\boldsymbol{I}^*_7$ presented for new origins of ellipses for $\boldsymbol{U}^*_5$ influence ("2" and "3" on Figure 8) would provide good accuracy for including more supply voltage harmonic influence components.

The presentation in Figure 8 allows to propose that the harmonic current $\boldsymbol{I}^*_x$ components, determined respectively

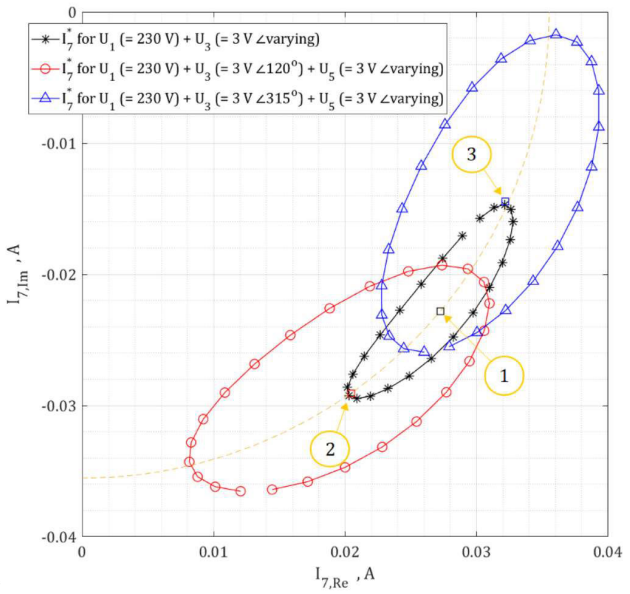

FIGURE 8. Explanation on harmonic current I_{*7} cumulative products results with $U_1 = 230$ V; U_3 and $U_5 = 3$ V. Red line: $\varphi_{U3} = 105°$, blue line: $\varphi_{U3} = 300°$, φ_{U5} phase values 0,15,30…345, plot of measured response.

TABLE 11. Harmonic Voltage Levels and Phase Ange Present in Residential grid, Flat and Pointed Top Waveforms.

	U^*_1	U^*_3		U^*_5		U^*_7		U^*_9	
	U_1 , V	U_3 , V	φ_{U3} °	U_5 , V	φ_{U5} °	U_7 , V	φ_{U7} °	U_9 , V	φ_{U9} °
Grid-1	230	0.35	51	1.0	224	0.97	15	0	0
Grid-2	230	0.15	80	1.6	296	0.79	37	0	0
Flat top	230	5.5	0	3.8	180	2.0	0	0.57	180
Pointed top	230	6.6	0	4.7	180	1.4	180	0	0

with (10) for each supply voltage harmonic component $\boldsymbol{U}^*_y$ influence individually would be presenting the cumulation in a linear summation as

$$\Delta I_x = \sum_{n=1;y=2n+1}^{N} \Delta I_{x,y} \tag{27}$$

$$\Delta \varphi_{Ix} = \sum_{n=1;y=2n+1}^{N} \Delta \varphi_{Ix,y} \tag{28}$$

where N is the number of odd harmonic components considered. The (27) and (28) are basically subsets of the matrix evaluation provided in (11 – 14). However, the authors express that this cumulation approach should be used with care, as this is providing good accuracy generally for supply voltage harmonics low magnitude levels. For example, the linear relation could be used with voltage harmonics levels of up to 1.5 V, while greater supply voltage harmonic levels would provide a remarkable additional deviation. This can be traced to additional G_{xy} and K_{xy} dependence on the $\boldsymbol{I}^*_x$ ellipse cumulative base point positioning. The authors intend to present work on the stated cumulative $\boldsymbol{I}^*_x$ calculation model in the future.

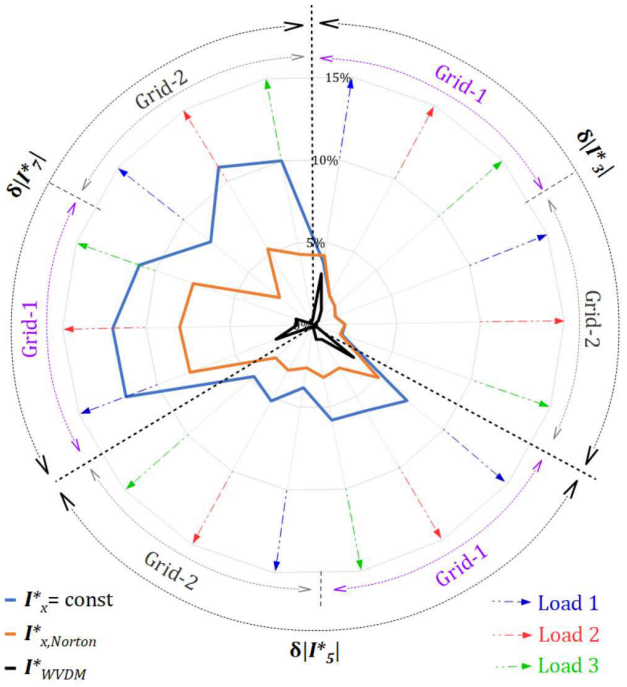

FIGURE 9. Deviation in magnitude between measurements and modelled (constant-current, Norton, proposed model) values, for two residential-area grid waveforms.

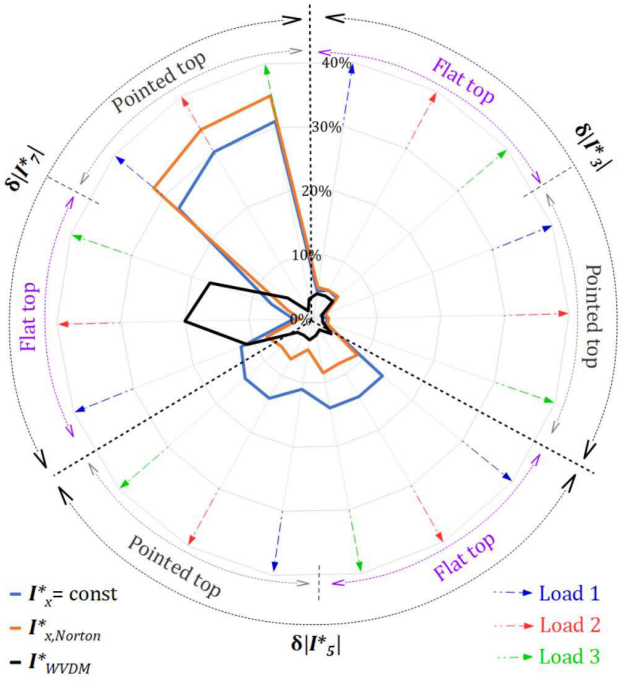

FIGURE 10. Deviation in magnitude between measurements and modelled (constant-current, Norton, proposed model) values, for Flat and pointed-top supply waveforms.

IX. VALIDATION OF PROPOSED MODEL

Even though stating the expected limitations to the cumulative harmonic current evaluation in the previous chapter, the linear cumulative $\boldsymbol{I}^*_x$ model can be seen to provide

TABLE 12. Difference of Estimations and Measurement for tested residential and industrial voltage supply waveform.

Load	Waveform type	Estimation technique	Difference					
			% $\delta\|I^*_3\|$	$\delta\varphi_{I3}$	% $\delta\|I^*_5\|$	$\delta\varphi_{I5}$	% $\delta\|I^*_7\|$	$\delta\varphi_{I7}$
1	Grid-1	I^*_x = const	3.8	<1	7.2	1	12	3
		$I^*_{x,Norton}$	4.2	<1	5.0	2	7.9	4
		I^*_{WVDM}	3.1	1	3.1	2	2.4	3
	Grid-2	I^*_x = const	1.4	5	3.8	8	7.9	11
		$I^*_{x,Norton}$	1.4	5	2.6	<1	2.6	14
		I^*_{WVDM}	0.1	<1	0.1	1	0.1	2
	Flat top	I^*_x = const	4.3	20	14	40	12	65
		$I^*_{x,Norton}$	4.9	14	9.0	25	7.7	48
		I^*_{WVDM}	3.9	<1	3.7	3	12	9
	Pointed top	I^*_x = const	1.3	15	12	27	28	44
		$I^*_{x,Norton}$	2.1	8	4.8	8	33	53
		I^*_{WVDM}	1.5	1	3.3	2	5.1	5
2	Grid-1	I^*_x = const	2.0	1	6.0	3	12	7
		$I^*_{x,Norton}$	2.0	2	3.0	3	8.0	<1
		I^*_{WVDM}	1.0	<1	1	<1	1.0	<1
	Grid-2	I^*_x = const	1.9	5	5.2	7	11	9
		$I^*_{x,Norton}$	1.9	4	3.1	<1	5.3	12
		I^*_{WVDM}	0.2	<1	0.2	1	0.3	2
	Flat top	I^*_x = const	5.0	18	14	38	3.0	63
		$I^*_{x,Norton}$	5.0	12	8.0	22	2.0	47
		I^*_{WVDM}	4.0	2	2.0	1	20	3
	Pointed top	I^*_x = const	2.3	16	15	30	30	51
		$I^*_{x,Norton}$	2.5	8	7.1	10.	34	61
		I^*_{WVDM}	1.5	<1	2.9	2	1.4	6
3	Grid-1	I^*_x = const	1.7	1	5.8	3	12	7
		$I^*_{x,Norton}$	1.7	2	3.2	3	7.6	<1
		I^*_{WVDM}	0.4	<1	0.9	<1	1.1	<1
	Grid-2	I^*_x = const	1.8	5	4.7	8	10	9
		$I^*_{x,Norton}$	1.7	4	3.0	<1	4.3	13
		I^*_{WVDM}	0.1	<1	0.2	1	0.3	2
	Flat top	I^*_x = const	4.9	19	14	38	6.8	64
		$I^*_{x,Norton}$	5.2	12	8.5	23	4.2	47
		I^*_{WVDM}	4.1	2	2.6	2	17	6
	Pointed top	I^*_x = const	2.1	16	14	29	31	48
		$I^*_{x,Norton}$	2.4	8	6.5	9	35	58
		I^*_{WVDM}	1.6	<1	3.2	2	3.1	6

considerably improved performance and accuracy compared to the previously available models. In order to present this, specific waveforms listed in Table 11 will be used.

As the residential grid supply tend to have small harmonic magnitudes, the resultant load current harmonics have nonlinear part insignificant as compared to linear part. More extreme cases are available in the industrial grids, where ''pointed and flat-top'' supply voltage waveform could emerge more often. The latter exceed the proposed model accuracy range; however, could be used for reference of different model presentations.

For load current harmonic fingerprint estimation using the proposed model, 2 recorded residential grid voltage waveforms have been used (Grid-1 and Grid-2, in Table 11). Similarly, but for more extensive industrial case presentation through ''flat top'' and ''pointed top'' waveforms are presented only as reference (Table 11).

For the loads discussed in the previous chapters, the measurements were carried out as the loads were supplied the waveforms in question, using similar grounds as (chapter II).

Table 12 depicts the measurement and proposed model estimation accuracy comparison of different techniques by modeling response of the loads for the targeted waveforms using (11 – 14). The deviation in harmonic currents magnitude $\delta|\boldsymbol{I}^*_h|$ is presented for different harmonic models (see also Figure 9 and 10). The constant harmonic current injection ($\boldsymbol{I}^*_x$ = const) and Norton model ($\boldsymbol{I}^*_{x,Norton}$) waveforms have been compared; the proposed model ($\boldsymbol{I}^*_{x,WVDM}$) presents considerable accuracy improvement. Table 12 readings have been compared to on Figures 9 – 10 for the magnitude result analysis. It has to be noted, that the phase angle values for all considered $\boldsymbol{I}^*_x$ observed, are presenting less than 10° difference compared to the measured values. Figure 11 presents the comparison of load current harmonic measurements and modeled response of different harmonic modeling

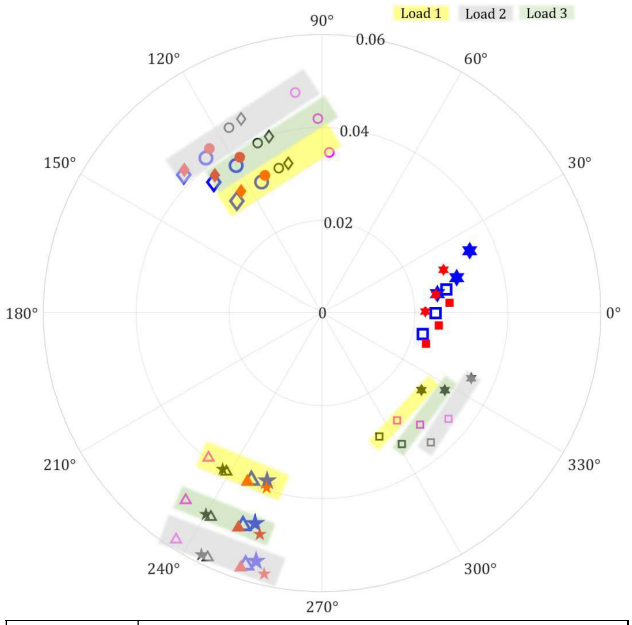

Waveform	Current harmonics		
Pure sine	△ $I^*_{3,Base}$	○ $I^*_{5,Base}$	□ $I^*_{7,Base}$
Flat top	△ $I^*_{3,Meas\_FT}$	○ $I^*_{5,Meas\_FT}$	□ $I^*_{7,Meas\_FT}$
	△ $I^*_{3,Norton\_FT}$	○ $I^*_{5,Norton\_FT}$	□ $I^*_{7,Norton\_FT}$
	▲ $I^*_{3,WVDM\_FT}$	● $I^*_{5,WVDM\_FT}$	■ $I^*_{7,WVDM\_FT}$
Pointed top	★ $I^*_{3,Meas\_PT}$	◇ $I^*_{5,Meas\_PT}$	✸ $I^*_{7,Meas\_PT}$
	★ $I^*_{3,Norton\_PT}$	◇ $I^*_{5,Norton\_PT}$	✸ $I^*_{7,Norton\_PT}$
	★ $I^*_{3,WVDM\_PT}$	◆ $I^*_{5,WVDM\_PT}$	✸ $I^*_{7,WVDM\_PT}$

FIGURE 11. Comparison of load current harmonic measurements and modeled response of different harmonic modeling techniques, for flat-top (FT) and pointed-top (PT) voltage waveforms (see Table 12).

techniques, for flat-top (FT) and pointed-top (PT) voltage waveforms.

The proposed model harmonic current estimation is rather usable even for the industrial cases presented, however this is not valid for all industrial waveform presentations. The phase margin tends to present more accurate estimation outcome, result of improved phase results due to cross-order harmonic coupling evaluation.

X. CONCLUSION

In the presentation above, a novel approach to model the supply voltage harmonics effect to load current of a non-linear load presented very good outcome and correspondence of measured harmonic current levels and phase angles. The type A LED presents a solid example for this model, given the excellent correlation between the time-domain initiation moment shift derived harmonic phase angle variations. In previous network modeling techniques such as Norton equivalent model, the consideration of cross-order harmonic influence for current and voltage is not available, however, this makes up a significant proportion to, for example, 7th harmonic current estimation. Frequency coupling matrix modeling contains many admittance matrix parameters to account cross-order coupling, however the results provide considerable deviations and no physical ground to the emergence of cross-order coupling. The proposed timed-domain waveform variation defined model provides a detailed understanding of the interaction between the supply voltage and current harmonics variations and their cross-order coupling.

Nevertheless, authors point out that the linearity assumption in the harmonic current components cumulative assessment has narrow application span. The discussed lower order harmonics' model is acceptable until ∼1.5 V of supply voltage harmonic levels used. In order to improve this model accuracy, a non-linear approach would be needed for the total harmonic current calculation. The present model, however, has been verified to provide good outcome for residential grid supply voltage harmonic cases. The use of this linear model would be especially feasible for residential harmonic current level estimation, where the harmonic vectors are considered. Authors aim to address the cumulative multiple influencer modelling with accurate nonlinear part estimation details in future publications.

REFERENCES

[1] I. Santiago, M. A. López-Rodríguez, A. Gil-de-Castro, A. Moreno-Munoz, and J. J. Luna-Rodríguez, "Energy consumption of audiovisual devices in the residential sector: Economic impact of harmonic losses," *Energy*, vol. 60, pp. 292–301, Oct. 2013, doi: 10.1016/j.energy.2013.08.018.

[2] T. Vinnal, M. Jarkovoi, and L. Kutt, "Harmonic currents and voltages in LV networks of Estonia: Measurement results, case studies," in *Proc. IEEE 59th Int. Sci. Conf. Power Electr. Eng. Riga Tech. Univ. (RTUCON)*, Nov. 2018, pp. 1–7, doi: 10.1109/RTUCON.2018.8659875.

[3] *Electromagnetic Compatibility (EMC)—Part 3-2: Limits—Limits for Harmonic Current Emissions (Equipment Input Current 16 A Per Phase)*, Standard IEC 61000-3-2:2018, 2018.

[4] N. Shabbir, L. Kütt, M. Jarkovoi, M. N. Iqbal, A. Rassõlkin, and K. Daniel, "An overview of measurement standards for power quality," *Agron. Res.*, vol. 19, no. 1, pp. 944–960, 2021, doi: 10.15159/AR.21.074.

[5] X. Xu, A. J. Collin, S. Z. Djokic, S. Yanchenko, F. Möller, J. Meyer, R. Langella, and A. Testa, "Analysis and modelling of power-dependent harmonic characteristics of modern PE devices in LV networks," *IEEE Trans. Power Del.*, vol. 32, no. 2, pp. 1014–1023, Apr. 2017, doi: 10.1109/TPWRD.2016.2574566.

[6] P. W. Lehn and K. L. Lian, "Frequency coupling matrix of a voltage-source converter derived from piecewise linear differential equations," *IEEE Trans. Power Del.*, vol. 22, no. 3, pp. 1603–1612, Jul. 2007, doi: 10.1109/TPWRD.2006.886779.

[7] M. N. Iqbal, L. Kutt, B. Asad, and N. Shabbir, "Impact of cable impedance on the harmonic emission of LED lamps," in *Proc. 21st Int. Sci. Conf. Electric Power Eng. (EPE)*, Oct. 2020, pp. 1–6, doi: 10.1109/EPE51172.2020.9269271.

[8] A. Gil-De-Castro, R. Medina-Gracia, S. K. Ronnberg, A. M. Blanco, and J. Meyer, "Differences in the performance between CFL and LED lamps under different voltage distortions," in *Proc. 18th Int. Conf. Harmon. Quality Power (ICHQP)*, May 2018, pp. 1–6, doi: 10.1109/ICHQP.2018.8378918.

[9] L. Kutt, E. Saarijarvi, M. Lehtonen, H. Molder, and J. Niitsoo, "Estimating the harmonic distortions in a distribution network supplying EV charging load using practical source data—Case example," in *Proc. IEEE Power Energy Soc. Gen. Meeting*, Oct. 2014, pp. 4–8, doi: 10.1109/PESGM.2014.6939267.

[10] A. J. Collin, X. Xu, S. Z. Djokic, F. Moller, J. Meyer, L. Kutt, and M. Lehtonen, "Survey of harmonic emission of electrical vehicle chargers in the European market," in *Proc. Int. Symp. Power Electron., Electr. Drives, Autom. Motion (SPEEDAM)*, Jun. 2016, pp. 1208–1213, doi: 10.1109/SPEEDAM.2016.7526005.

[11] A. Kalair, N. Abas, A. R. Kalair, Z. Saleem, and N. Khan, "Review of harmonic analysis, modeling and mitigation techniques," *Renew. Sustain. Energy Rev.*, vol. 78, pp. 1152–1187, Oct. 2017, doi: 10.1016/j.rser.2017.04.121.

[12] A. Taghvaie, F. Zare, R. Sharma, and D. Kumar, "Impacts of grid impedance on power quality of converters in distribution networks," in *Proc. 48th Annu. Conf. IEEE Ind. Electron. Soc. (IECON)*, Oct. 2022, pp. 1–6, doi: 10.1109/IECON49645.2022.9968362.
[13] H. Rathnayake, K. G. Khajeh, F. Zare, and R. Sharma, "Harmonic analysis of grid-tied active front end inverters for the frequency range of 0-9 kHz in distribution networks: Addressing future regulations," in *Proc. IEEE Int. Conf. Ind. Technol. (ICIT)*, Feb. 2019, pp. 446–451, doi: 10.1109/ICIT.2019.8755015.
[14] J. Yadav, K. Vasudevan, J. Meyer, and D. Kumar, "Frequency coupling matrix model of a three-phase variable frequency drive," *IEEE Trans. Ind. Appl.*, vol. 58, no. 3, pp. 3652–3663, May 2022, doi: 10.1109/TIA.2022.3156104.
[15] J. Yadav, K. Vasudevan, J. Meyer, and D. Kumar, "Modelling three phase variable frequency drive using a frequency coupling matrix," in *Proc. IEEE 1st Int. Conf. Smart Technol. Power, Energy Control (STPEC)*, Sep. 2020, pp. 1–6, doi: 10.1109/STPEC49749.2020.9297761.
[16] Y. Xiao and X. Yang, "Harmonic summation and assessment based on probability distribution," *IEEE Trans. Power Del.*, vol. 27, no. 2, pp. 1030–1032, Apr. 2012, doi: 10.1109/TPWRD.2012.2187124.
[17] R. Savoor and K. Meier-Hellstern, "Estimating the frequency coupling matrix from network measurements," *IEEE Trans. Control Netw. Syst.*, vol. 7, no. 2, pp. 353–388, Sep. 2020, doi: 10.1201/9781315208787-16.
[18] R. Langella, A. Testa, J. E. Caicedo, A. A. Romero, H. C. Zini, J. Meyer, and N. R. Watson, "On the use of Fourier descriptors for the assessment of frequency coupling matrices of power electronic devices," in *Proc. 18th Int. Conf. Harmon. Quality Power (ICHQP)*, May 2018, pp. 1–6, doi: 10.1109/ICHQP.2018.8378908.
[19] K. J. Son, G. S. An, K. D. Nam, and T. G. Chang, "An advanced frequency estimation algorithm based on analytic compensation of effects of dominant harmonic in power systems," *IEEE Access*, vol. 9, pp. 146568–146577, 2021, doi: 10.1109/ACCESS.2021.3122469.
[20] Y. Sun, G. Zhang, W. Xu, and J. G. Mayordomo, "A harmonically coupled admittance matrix model for AC/DC converters," *IEEE Trans. Power Syst.*, vol. 22, no. 4, pp. 1574–1582, Nov. 2007, doi: 10.1109/TPWRS.2007.907514.
[21] L. F. Beites, J. G. Mayordomo, and X. Yang, "The harmonically coupled admittance matrix of the single-phase diode rectifier," *IEEE Access*, vol. 9, pp. 128023–128031, 2021, doi: 10.1109/ACCESS.2021.3110597.
[22] K. Daniel, L. Kutt, M. N. Iqbal, N. Shabbir, and M. Jarkovoi, "Description of practical load harmonic current emission due to voltage harmonic variation," in *Proc. IEEE 62nd Int. Sci. Conf. Power Electr. Eng. Riga Tech. Univ. (RTUCON)*, Nov. 2021, pp. 1–6, doi: 10.1109/RTUCON53541.2021.9711594.
[23] M. Ramzan, A. Othman, and N. R. Watson, "Accurate harmonic analysis of distribution systems," in *Proc. 7th IEEE Workshop Electron. Grid (eGRID)*, Nov. 2022, pp. 1–5, doi: 10.1109/eGRID57376.2022.9990007.
[24] M. N. Iqbal, L. Kütt, B. Asad, N. Shabbir, and I. Rasheed, "Time-dependent variations in current harmonic emission by LED lamps in the low-voltage network," *Electr. Eng.*, vol. 103, no. 3, pp. 1525–1539, Jun. 2021, doi: 10.1007/s00202-020-01175-4.
[25] D. Gallo, R. Langella, M. Luiso, A. Testa, and N. R. Watson, "A new test procedure to measure power electronic devices' frequency coupling admittance," *IEEE Trans. Instrum. Meas.*, vol. 67, no. 10, pp. 2401–2409, Oct. 2018, doi: 10.1109/TIM.2018.2819318.
[26] M. N. Iqbal, L. Kutt, N. Shabbir, and B. Asad, "Comparison of current harmonic emission by different lighting technologies," in *Proc. IEEE 61th Int. Sci. Conf. Power Electr. Eng. Riga Tech. Univ. (RTUCON)*, Nov. 2020, pp. 1–5, doi: 10.1109/RTUCON51174.2020.9316615.
[27] M. N. Iqbal, L. Kütt, K. Daniel, M. Jarkovoi, B. Asad, and N. Shabbir, "Bivariate stochastic model of current harmonic analysis in the low voltage distribution grid," *Proc. Est. Acad. Sci.*, vol. 70, no. 2, pp. 190–206, 2021, doi: 10.3176/proc.2021.2.08.
[28] M. N. Iqbal, L. Kütt, B. Asad, T. Vaimann, A. Rassõlkin, and G. L. Demidova, "Time dependency of current harmonics for switch-mode power supplies," *Appl. Sci.*, vol. 10, no. 21, pp. 1–12, 2020, doi: 10.3390/app10217806.
[29] M. N. Iqbal, M. Jarkovoi, L. Kutt, and N. Shabbir, "Impact of LED thermal stability to household lighting harmonic load current modeling," in *Proc. Electr. Power Quality Supply Rel. Conf. (PQ) Symp. Electr. Eng. Mechatronics (SEEM)*, Jun. 2019, pp. 1–6, doi: 10.1109/PQ.2019.8818226.
[30] M. N. Iqbal, "Measurement based approach for residential customer stochastic current harmonic modelling," Ph.D. dissertation, Tallinn Univ. Technol., Tallinn, Estonia, Tech. Rep. 43/2021, doi: 10.23658/taltech.43/2021.
[31] J. Cunill-Solà and M. Salichs, "Study and characterization of waveforms from low-watt (≪25 W) compact fluorescent lamps with electronic ballasts," *IEEE Trans. Power Del.*, vol. 22, no. 4, pp. 2305–2311, Oct. 2007.
[32] D. Chakravorty, J. Meyer, P. Schegner, S. Yanchenko, and M. Schocke, "Impact of modern electronic equipment on the assessment of network harmonic impedance," *IEEE Trans. Smart Grid*, vol. 8, no. 1, pp. 382–390, Jan. 2017, doi: 10.1109/TSG.2016.2587120.
[33] A. J. Collin, S. Z. Djokic, J. Drapela, Z. Guo, R. Langella, A. Testa, and Neville . R. Watson, "Analysis of approaches for modeling the low frequency emission of LED lamps," *Energies*, vol. 13, no. 7, pp. 1–33, 2020, doi: 10.3390/en13071571.
[34] J. Molina and L. Sainz, "Compact fluorescent lamp modeling for large-scale harmonic penetration studies," *IEEE Trans. Power Del.*, vol. 30, no. 3, pp. 1523–1531, Jun. 2015, doi: 10.1109/TPWRD.2014.2363143.
[35] A. Alduraibi, J. Yaghoobi, and F. Zare, "Impacts of grid voltage harmonics amplitude and phase angle values on power converters in distribution networks," *IEEE Access*, vol. 9, pp. 92017–92029, 2021, doi: 10.1109/ACCESS.2021.3093026.
[36] J. Drapela, R. Langella, A. Testa, and V. Vendemia, "A new analytical model of single-phase diode bridge rectifiers in the presence of interharmonics in supply voltage," *IEEE Open Access J. Power Energy*, early access, Feb. 13, 2023, doi: 10.1109/OAJPE.2023.3244330.
[37] J. Kwon, X. Wang, F. Blaabjerg, C. L. Bak, A. R. Wood, and N. R. Watson, "Harmonic instability analysis of a single-phase grid-connected converter using a harmonic state-space modeling method," *IEEE Trans. Ind. Appl.*, vol. 52, no. 5, pp. 4188–4200, Sep./Oct. 2016, doi: 10.1109/TIA.2016.2581154.
[38] D. Kumar and F. Zare, "Harmonic analysis of grid connected power electronic systems in low voltage distribution networks," *IEEE Trans. Emerg. Sel. Topics Power Electron.*, vol. 4, no. 1, pp. 70–79, Mar. 2016, doi: 10.1109/JESTPE.2015.2454537.

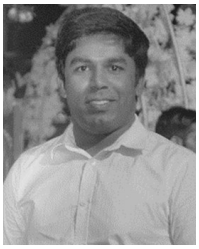

KAMRAN DANIEL (Graduate Student Member, IEEE) received the B.Sc. degree in electronics engineering from The Islamia University of Bahawalpur, in 2008, and the M.S. degree from the University of South Asia, Lahore, Pakistan. He is currently pursuing the Ph.D. degree with the Tallinn University of Technology, Estonia. He is a Lecturer with the University of Engineering and Technology at Lahore. His research interests include network harmonic modeling, power line diagnostics, power quality, and electromagnetic compatibility.

LAURI KÜTT (Senior Member, IEEE) received the B.Sc. degree in computer and automation technology and the M.Sc. degree in electrical power engineering from the Tallinn University of Technology, Tallinn, Estonia, in 2002 and 2004, respectively, and the Ph.D. degree from the Department of Energy and Geotechnology, Tallinn University of Technology, in 2012. He is currently a Professor with the Department of Electrical Power Engineering and Mechatronics, Tallinn University of Technology. His current research interests include fast transients on electric power lines, power line diagnostics, power quality, and electromagnetic compatibility.

MUHAMMAD NAVEED IQBAL received the B.Sc. degree in electronics engineering from The Islamia University of Bahawalpur, Pakistan, in 2008, the M.S. degree from the University of New South Wales, Australia, in 2010, and the Ph.D. degree from the Department of Electrical Power Engineering and Mechatronics, Tallinn University of Technology, Estonia, in 2021. He is currently an Assistant Professor with the Department of Electrical Engineering, Government College University Lahore, Pakistan. His current research interests include power line diagnostics, power quality, and electromagnetic compatibility.

NOMAN SHABBIR (Senior Member, IEEE) received the B.S. degree in computer engineering from COMSATS, Lahore, Pakistan, and the M.S. degree in electrical engineering from BTH, Sweden. He is currently a Research Fellow with the FinEST Center for Smart Cities, Tallinn University of Technology, Estonia. He is also an Assistant Professor with GC University Lahore, Pakistan. His research interests include renewable energy systems, smart grids, machine learning, and ICT.

MARTIN PARKER received the B.Sc. and M.Sc. degrees in mechatronics from the Tallinn University of Technology, in 2011 and 2013, respectively. He is currently a Junior Researcher with the Department of Electrical Power Engineering and Mechatronics, Tallinn University of Technology. His current research interests include metrology, measurement instrumentation, and lighting technologies.

MAREK JARKOVOI received the M.Sc. (Hons.) and Ph.D. degrees from the Tallinn University of Technology, in 2013 and 2019, respectively. He is currently an Engineer, a Researcher, and an Electronics Development Engineer with the Tallinn University of Technology. He is an expert in areas on measurement models and methods. His current research interests include applied electromagnetics and electromagnetic compatibility and electric power quality, focused on harmonic distortions.